A NUMERICAL AND EXPERIMENTAL APPROACH FOR MODELING POROSITY DUE TO ENTRAPPED AIR AND VOLATILES OFF-GASSING DURING MANUFACTURING OF COMPOSITE STRUCTURES

Curtis Hickmott[1], Alireza Forghani[1], Victoria Hutten[1], Evan Lorbiecki[1], Frank Palmieri[2], Brian Grimsley[2], Brian Coxon[1], Goran Fernlund[1,3], Anoush Poursartip[1,3]

[1] Convergent Manufacturing Technologies US, Seattle, WA
[2] NASA Langley Research Center, Hampton, VA
[3] Department of Materials Engineering, The University of British Columbia, Vancouver, BC, Canada

ABSTRACT

High performance composite structures have strict requirements regarding acceptable levels of porosity. The impact can be significant on mechanical performance and mitigating the growth of voids can be a challenge given the complexity of the problem. The evolution of porosity can be summarized as a balance between sources and sinks which determine void growth or shrinkage. The primary sources of void growth include bag leaks, entrapped air in the system, off-gassing of volatiles, and cure shrinkage. Mechanisms which mitigate porosity include removal of air from the system and maintaining sufficient resin pressure during the process to keep volatiles in solution. In this paper, an approach for modeling the evolution of voids due to entrapped air and volatiles is presented. It has been shown in previous experimental studies that decreases in local resin pressure are linked to a higher likelihood of porosity formation. Results of the study are compared to experiments in which the local resin pressure was measured and micrographs of the panels were taken to characterize the porosity.

1. INTRODUCTION

Composite performance requirements restrict the process windows for manufacturing of aerospace-grade carbon fiber reinforced polymer (CFRP) prepregs cured in autoclaves in order to manage the formation of key defects. One of the primary defects of interest is porosity as it has been shown to affect the performance of the structural components subjected to both in-service and ultimate loading conditions. The major sources of porosity include bag leaks, entrapped air in the system, off-gassing of volatiles, and cure shrinkage. In order to minimize these sources, sufficient time must be allowed for air to evacuate the system. Maintaining an adequate resin pressure throughout the process provides restraint on void growth due to volatiles [1, 2]. In previous work, local resin pressure has been shown to indicate the likelihood of porosity and a physics-based model has been demonstrated to predict resin pressure [3, 4]. The focus of this article is to extend this modeling capability to include the off-gassing of volatiles and compare to experimental data. Currently the modeling framework discussed in this paper can simulate the evolution of porosity in a composite laminate based on contributions from entrapped gas and the off-gassing of volatiles and provide a void volume fraction for each source.

The scope of this research includes autoclave cure of thermosetting prepreg materials. Different stages of the manufacturing process can contribute to formation of porosity. The material is first deposited and often debulked. During this stage, air can become entrapped between plies and sometimes removed by evacuation via channels that remain open. As the material is heated and pressure is applied in the autoclave, the gas evacuation channels will close when the resin viscosity becomes sufficiently low enough to flow. At this point, entrapped gas is often difficult to remove from the system. As the temperature continues to increase, the vapor pressure of the moisture (or other volatiles) in the resin increases, driving porosity formation unless the resin pressure remains above the critical pressure threshold. As cure continues to advance, resin cure shrinkage takes place. Depending on the surrounding constraints of the system, fiber volume fraction (V_f), viscosity, and tensile stresses formed in the matrix due to shrinkage can lead to formation of *tearing* or microcracking after gelation.

The focus of this paper is the inclusion of a quantitative model for the prediction of volatiles and off-gassing to a modeling framework which already supports the transport of resin and gas through a fiber bed while tracking changing material properties.

1.1 Model Development

The modeling framework discussed in the paper is an extension of work described in previous articles by the authors [3, 4]. It has been demonstrated that the concepts of poroelasticity (originally developed to model consolidation of soils) can be extended to model the pre-gelation regime of the composites manufacturing cure process where resin flows through the fiber bed (porous media) while undergoing chemical and physical changes [5].

Niaki and co-workers developed a poroelastic representation of the three-phase system comprising of fiber bed, liquid resin and gas to simulate the autoclave manufacturing process [6, 7]. This approach enables the prediction of key composite processing defects, specifically the evolution of voids and the final porosity. In order to accommodate current commercial off the shelf (COTS) finite element software tools which do not support a porous media with two independent pore fluids (gas and resin), the gas and resin pressure are assumed equal. This allows the governing equations to reduce to an equivalent hybrid fluid based on the saturation of the gas and resin phase [4].

Previous capabilities developed under the current program have included the prediction of gas transport through the system (viscous resin and fiber bed skeleton) and a qualitative likelihood of off-gassing. Recent developments have focused on modeling the kinetics of moisture off-gassing during the cure process. This mechanism can be summarized as the diffusion of moisture dissolved in the resin to voids and evaporation leading to void growth. Maintaining sufficient resin pressure can suppress the diffusion-driven bubble (porosity) growth.

1.2 Volatiles & Off-gassing Model Development

This mechanism assumes the predominant volatile is moisture and includes the diffusion of moisture into bubbles and the evaporation of that moisture shown schematically in Figure 1.

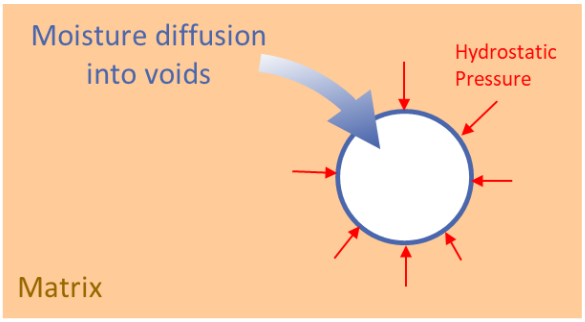

Figure 1. Schematic of volatiles and off-gassing mechanisms including the diffusion and evaporation of moisture

Diffusion of moisture is driven by the moisture concentration difference between the bubble surface (C_S) and in the resin (C_∞). If the concentration at the bubble surface is lower than the resin, moisture species will diffuse towards the bubble surface. Moisture concentration in the resin is expressed as a function of equilibrated relative humidity in the following form:

$$C_\infty = \frac{K_1 \rho_R}{W_R} (RH_0)^2$$

where ρ_R is the resin density and W_R is the resin weight fraction in the prepreg and K_1 is the solubility coefficient and RH_0 is the relative humidity of the environment under which equilibrium is achieved. Moisture concentration on the bubble surface takes the following form:

$$C_s = 4.061 \times 10^{-8} \frac{K_1 \rho_R}{W_R} \exp\left(\frac{9784}{T}\right) P_w^2$$

where P_w is the partial pressure of moisture in the bubble.

As discussed above, void growth will take place when C_∞ exceeds C_s. By equating C_∞ and C_s one can calculate the critical resin pressure, below which unstable void growth takes place.

$$P_{R,Critical} = 4.963E5 \, exp\left(-\frac{4892}{T}\right) RH_0 \quad \text{(in atm)}$$

Bubble Severity Index (BSI) is a scalar parameter defined as the ratio of the critical off-gassing pressure to resin pressure as shown below. A positive BSI means resin pressure is below critical off-gassing pressure, therefore it's likely for off-gassing to take place.

$$BSI = \frac{P_{R,Critical}}{P_R} - 1$$

In order to extend this framework to quantitatively capture the degree to which off-gassing occurs, simplifying assumptions are made which include:

- Moisture diffusion into bubble does not affect the moisture concentration in resin (C_∞)
- Surface tension on bubble surface is ignored

- Viscoelastic resistance from surrounding resin is ignored

Using the approach proposed by (Wood and Bader, 1994) [8, 9], steady state bubble growth due to moisture diffusion is defined as:

$$R^2 = R_0^2 + \frac{2DC_\infty}{\rho}(1 - \frac{1}{(1+BSI)^2})t$$

where *D* is the diffusion coefficient. The differential form in terms of porosity can be written as:

$$\frac{d\varphi}{\varphi_0} = \frac{3}{2}\frac{2DC_\infty RgT}{R_0^2 pM}\left(1 - \frac{1}{(1+BSI)^2}\right)\left[1 + \frac{2DC_\infty RgT}{R_0^2 pM}\left(1 - \frac{1}{(1+BSI)^2}\right)t\right]^{1/2} dt$$

In order to bring in the time dependency of the bubble growth due to the effect of resin viscosity, the concept of scaled time from viscoelasticity is employed:

$$\frac{d\varphi}{\varphi_0} = \frac{3DC_\infty RgT}{R_0^2 pM}\left(1 - \frac{1}{(1+BSI)^2}\right)\left[1 + \frac{2DC_\infty RgT}{R_0^2 pM}\left(1 - \frac{1}{(1+BSI)^2}\right)t^*\right]^{1/2} dt^*$$

$D = D(T)$: diffusion coefficient
C_∞: Resin moisture content
R_g: Ideal gas constant
T: Temperature in Kelvin
R_0: Initial bubble radius
BSI: Bubble Severity Index
dt^*: Scaled time increment defined as $\frac{1}{a^T}dt$
$a^T = a^T(\mu)$: the shift factor expressed as a function of resin viscosity

This off-gassing kinetics model is implemented in COMPRO's Integrated Flow-Stress (IFS3P*) simulation framework. Expansion of laminate due to off-gassing is simulated using free strains.

2. EXPERIMENTATION

To support validation of the modeling approach, a series of experiments has been performed on panels with a ply drop feature using a variety of caul sheet configurations. The ply drops combined with the caul sheet configurations drive pressure gradients in the laminates and resin flow. In addition, pressure shielded regions can form when the caul sheet compliance is insufficient at conforming to the laminate. The combination of these two phenomena is expected to drive variations in local resin pressure and influence the likelihood of off-gassing and porosity evolution. This work has been discussed previously and has been modeled after work performed at the University of British Columbia [10, 11].

2.1 Experimental Test Methodology

The test plan is shown below in Table 1, six panels were manufactured using a standard autoclave cure prepreg using three different caul sheets (one repeat for each configuration): thick caul (0.5 in, 12.7 mm), thin caul (0.125 in, 3.175 mm) and no caul sheet. Each panel was manufactured from Hexcel IM7/8552-1 CFRP prepreg into a 32 ply quasi-isotropic lay-up. Two plies were dropped every 1.27 cm (0.5 inch) in the transition region decreasing from 32 to 8 plies. The cure cycle used for these tests is shown in Figure 2.

Table 1. Test plan for caul sheet misfit panels

Test ID	Caul Thickness (cm)	Lay-up	Ply Drops (per 1.27 cm)	End Edge Dam	Autoclave Pressure psi (kPa)	Laminate Thickness (plies)	No. of Tests
1.1-1.2	No caul	Quasi-isotropic	2	Yes	85 (103 kPa)	32	2
2.1-2.2	0.32	Quasi-isotropic	2	Yes	85 (103 kPa)	32	2
3.1-3.2	1.27	Quasi-isotropic	2	Yes	85 (103 kPa)	32	2

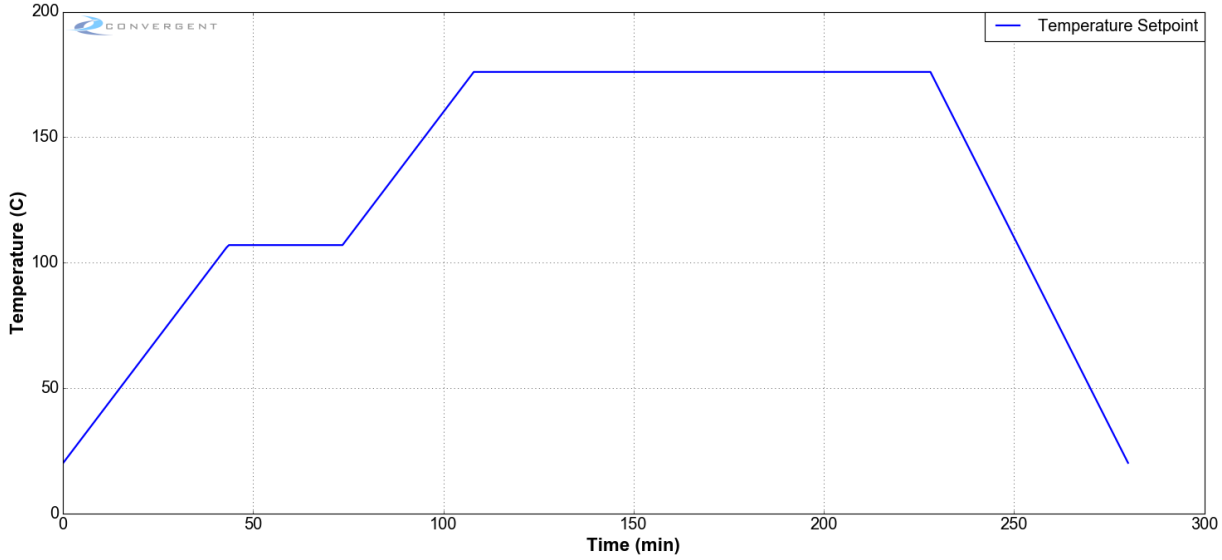

Figure 2. Caul sheet misfit panel cure cycle

To support comparison of the experimental work to simulations, the tooling was instrumented with local resin pressure sensors placed along the length of the laminate through the ply drops as shown in Figure 3. The panel is mirrored over the plane of symmetry to facilitate the pressure on the thin region of the panel which is due only to the deformation of the caul sheet.

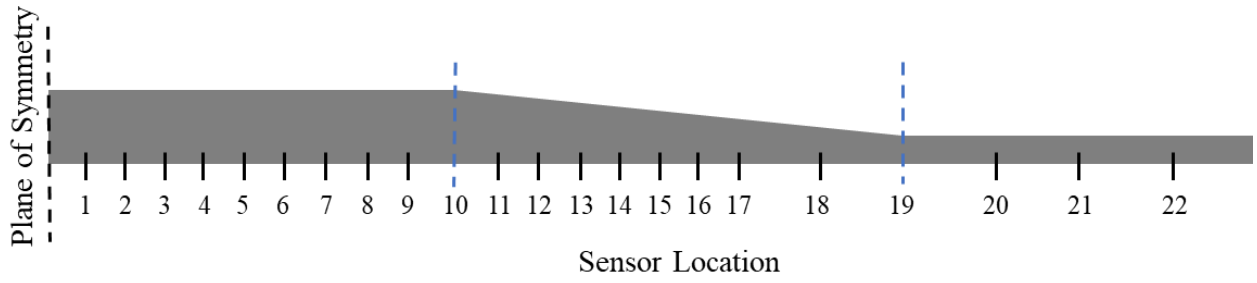

Figure 3. Schematic of the panel with ply drops and locations of the local resin pressure sensors

2.2 Experimental Results

Analysis of the experimental work has been performed using the data collected from resin pressure sensors and micrographs sectioned from the panels at strategic locations. Resin pressure data for the caul sheet misfit tests has been discussed in detail in previous work but is summarized below in order to evaluate against simulations enabled with the implemented off-gassing model. The resin pressure profiles for each of the six panels instrumented with sensors is shown below in Figure 4. Data is presented at minimum viscosity of the resin and the pressure gradient from the caul sheet against the ply drops will make resin flow most likely. The tests with no caul and the 0.32 cm (0.125 inch) caul show similar responses, the pressure is evenly distributed over the ply drop region. The vacuum bag conforms to the surface of the part as a baseline, the 0.32 cm (0.125 inch) caul sheet conforms to the surface as well. The 1.27 cm (0.5 inch) caul sheet shows a clear pressure gradient around the onset of ply drops, the caul sheet deforms under the pressure of the autoclave but is too stiff to contact the surface of the panel and creates local pressure peak followed by a region which is shielded from the pressure. This region of pressure shielding is the location of interest for likely void growth due to off-gassing.

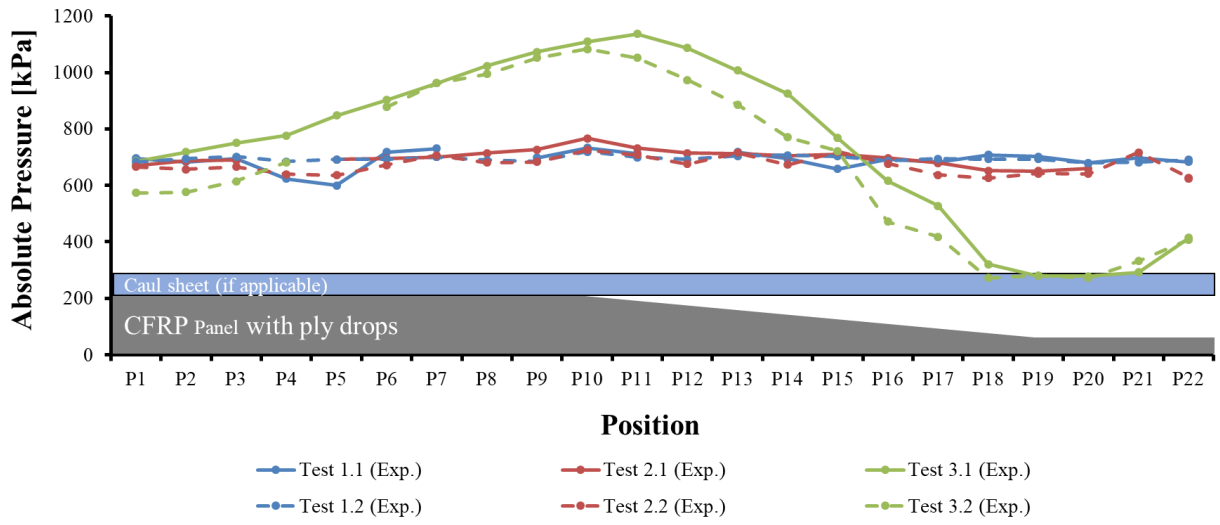

Figure 4. Resin pressure profiles along the 6 misfit panels with a schematic of the ply drop panel overlaid for reference (minimum viscosity), (data from failed sensors has been omitted)

2.2.1 Micrographs

Micrographs were sectioned from each panel at the locations of sensors P1, P11, and P19 (as shown in Figure 3). These locations were chosen as representative of the different conditions which might arise either in bagging or due to an improperly designed caul sheet. Representative micrographs for test 3.1 are shown below in Figure 5, the location of sensor P19 in the pressure shielded region displays higher porosity as expected. The lack of compliance in the caul sheet does not allow the pressure to drive gas evacuation out of the system and makes the region more susceptible to void growth as the vapor pressure of moisture increases. The two major sources of porosity discussed in this paper (entrapped air and volatiles) manifest in different stages in the cure process and via different mechanisms, an assumption made is that voids due to entrapped gas are predominantly interlaminar and voids due to off-gassing are predominantly found in the intralaminar layer or at a location where an initial defect (void) exists. Under this assumption, voids due to entrapped gas and off-gassing are observed in the available micrographs for test 3.1 and 3.2 at sensor P19.

ImageJ software has been used to analyze the void content in each micrograph and summarize the porosity observed at each location. Shown below in Figure 6 is the compiled data from the three test configurations (no caul, thin caul sheet, and thick caul sheet) at the three locations of interest (P1, P11, and P19). A threshold grayscale was defined for each image such that boundaries were clear around visible voids. The total void content per image was extracted for comparison, images were converted to a square area in order to allow cross comparison.

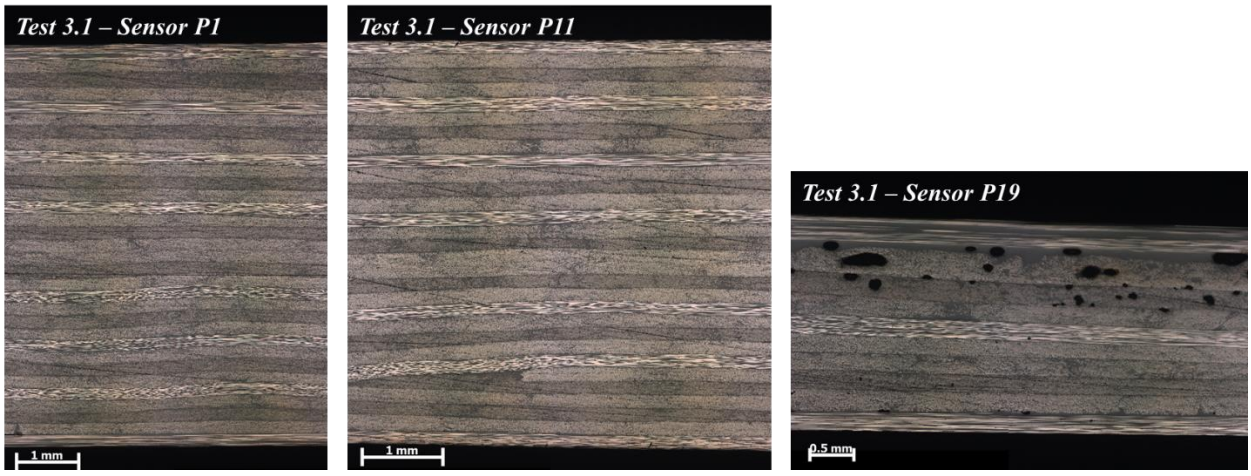

Figure 5. Representative micrographs from test 3.1 at the locations of sensors P1, P11, and P19 (from left to right)

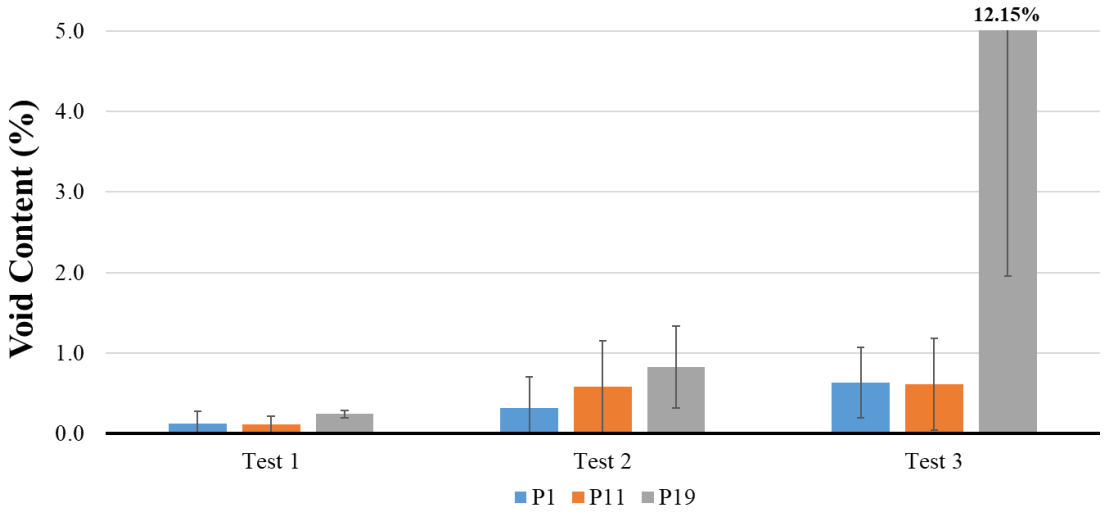

Figure 6. Void content per panel per location using image analysis (ImageJ)

3. NUMERICAL SIMULATIONS

Coupled thermal-consolidation simulations have been developed to replicate the experimental work discussed above. Simulations of each of the three configurations have been built in COMPRO-Abaqus 2018 under the Integrated Flow-Stress 3 Phase framework developed by Convergent Manufacturing Technologies. This approach provides the flow-compaction capabilities necessary to simulation resin and gas transport while updating the material properties with the cure.

3.1 Simulation Set-up

Simulations of the caul sheet misfit tests have been built including tooling and caul sheets (if applicable). The assembled models are shown below in Figure 7, additional simulation set up images will focus on the test 3.1 (thick caul sheet) but for the test with no caul sheet any boundary conditions discussed have been applied to the top surface of the part. To reduce computation time, only half of the panel and tooling have been simulated. A thermal analysis has been coupled with the flow-compaction analysis to allow thermal variation through the part and tooling. This approach allows the evolution of material properties such as degree of cure, and viscosity to be tracked throughout the part. Autoclave thermocouple (TC) data from each cure has been applied as a convective heat transfer boundary condition on the top and bottom surfaces of the system as shown in Figure 8. The autoclave pressure data was applied to the top surface of the caul sheet (or panel in the case of test 1.1). The pressure load and the boundary conditions in the model are shown in Figure 9.

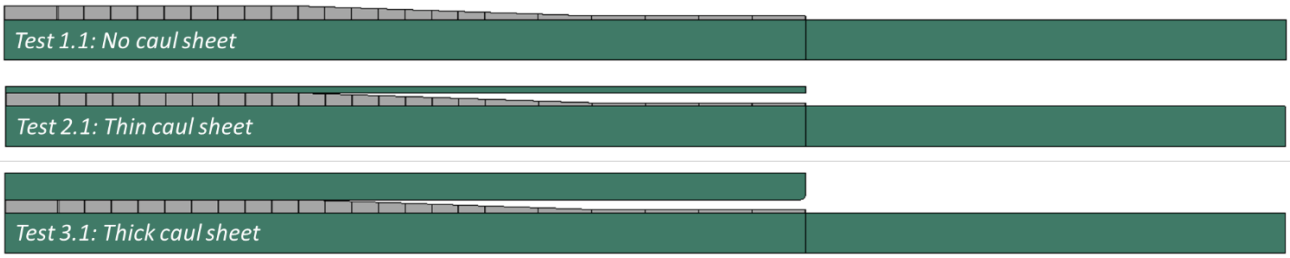

Figure 7. Images of the three caul sheet misfit simulation configurations

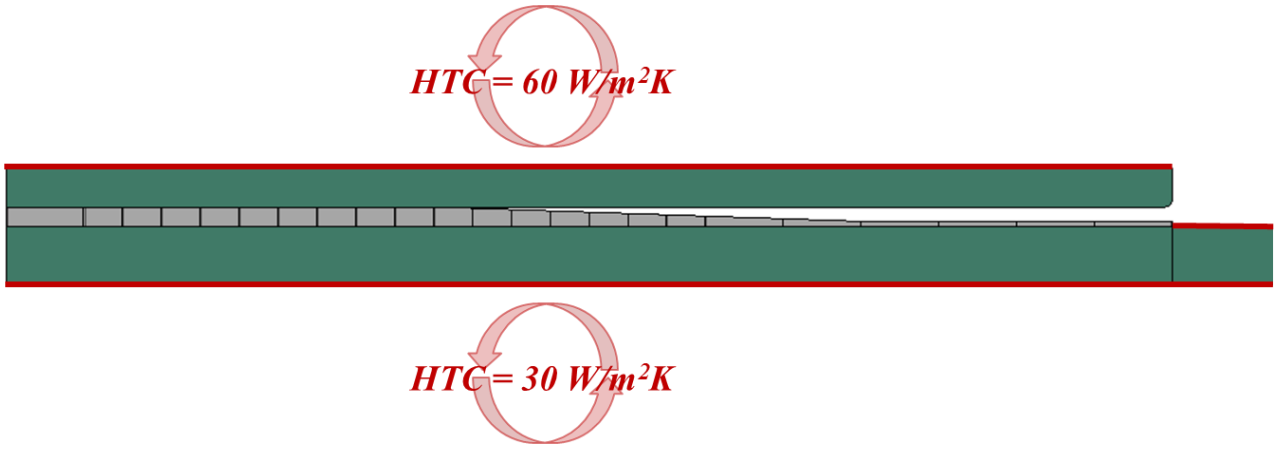

Figure 8. Image of the thermal boundary conditions applied to the model

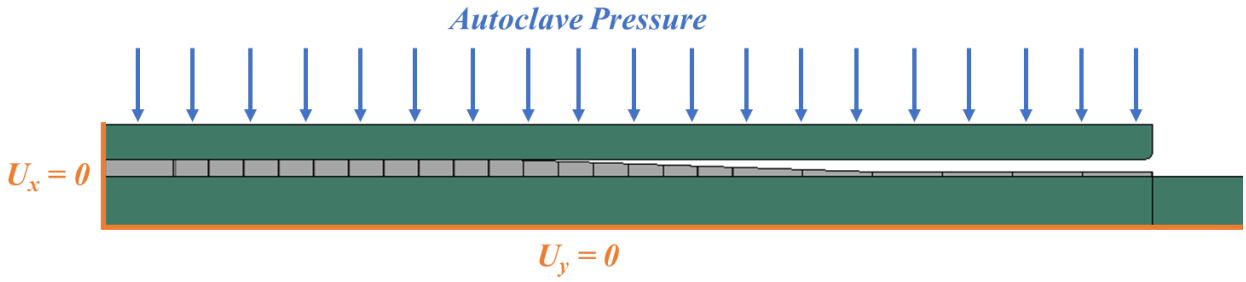

Figure 9. Image of the autoclave pressure load and boundary conditions applied

In order to support the new modeling features discussed in this article, additional input values are necessary for the modeling of gas transport, and off-gassing. Specifically, these parameters include the initial gas content (V_g), initial void fraction (V_v), and the relative humidity of the environment. The initial gas content reflects the gas trapped during the debulk stage and has been calculated based on measured thickness change in experimental tests. The initial void volume fraction is an assumed starting value in order to support the necessary calculations. The relative humidity of the environment influences the equilibrium moisture content of the panel. For example, a panel conditioned in an equilibrium relative humidity of 50% will have an equilibrium moisture content that is higher than a panel conditioned at 40% and thus more off-gassing may occur.

Table 2. Input parameters required for gas transport and off-gassing

Parameter	Input
Initial V_g (entrapped gas)	5.0%
Initial V_v (initial void content in resin)	0.1%
Relative humidity of the environment at equilibrium (RH_0)	40%

3.2 Simulation Results

Results of the simulations exercising the coupled thermal-flow compaction framework in COMPRO-Abaqus 2018 are presented below. Data comparing the experimental resin pressure to the predicted resin pressure profiles has been discussed in previous work by the authors, the evolution of gas transport and void growth is shown below. The contribution to void content from entrapped gas (solid lines) and the off-gassing of moisture (dashed lines) are shown below for three locations (P1, P11, and P19) which align with the locations of the micrographs discussed above. The contributions to porosity due to entrapped gas and volatiles for test 1, test 2, and test 3 are plotted below in Figure 10, Figure 11, and Figure 12. The scales for these graphs have been adjusted to reflect the range that porosity is predicted over. Local temperature and resin viscosity at P11 have been plotted for reference in the cure process.

The simulation for test 1 with no caul sheet exhibits no increase in void fraction due to off-gassing at any of the three locations shown as expected since this no-caul configuration leads to uniform pressure distribution along the part. The voids due to entrapped gas evacuate quickly in the early stages of pressure application as the evacuation pathways are still open and the mobility of gas is high. This evacuation slows down as the viscosity decreases and the pathways are closed.

In the simulation of test 2 (thin caul sheet) the evacuation has slowed significantly as a result of non-uniform application of pressure by the caul sheet. At location P19 which experiences pressure shielding, the initial entrapped air does not evacuate as there is no driving force from the caul sheet. Hot consolidation occurs when the resin viscosity has decreased and enables further thickness change and void collapse. In addition, some off-gassing is observed in the simulation at P19 due to pressure shielding.

The simulation of test 3 (thick caul sheet) shows wider variation over the range of locations discussed. The pressure shielded regions show no significant debulk/consolidation and are highly likely to exhibit off-gassing due to the low local resin pressure.

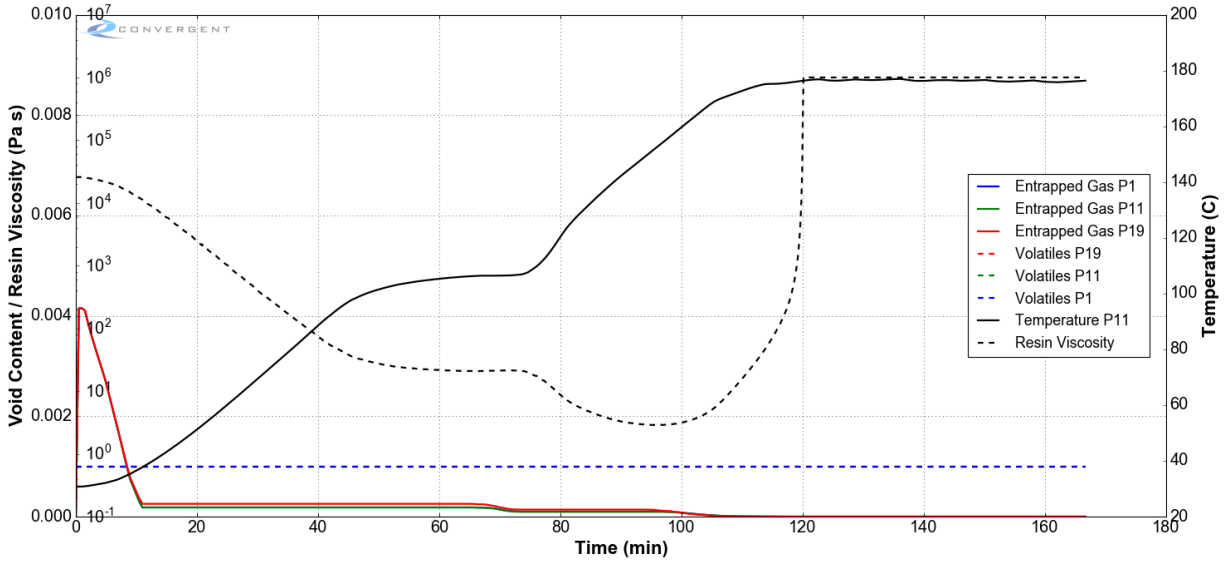

Figure 10. Evolution of the void content contributions in test 1 from entrapped gas (solid lines) and volatiles (dashed lines) over the representative sensors P1, P11, and P19

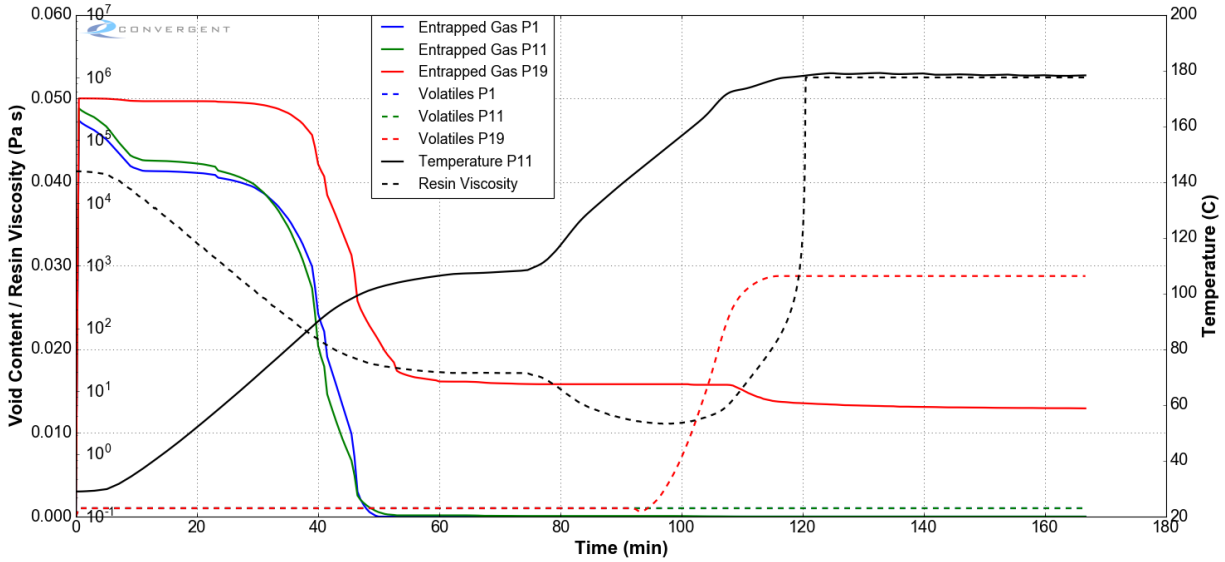

Figure 11. Evolution of the void content contributions in test 2 from entrapped gas (solid lines) and volatiles (dashed lines) over the representative sensors P1, P11, and P19

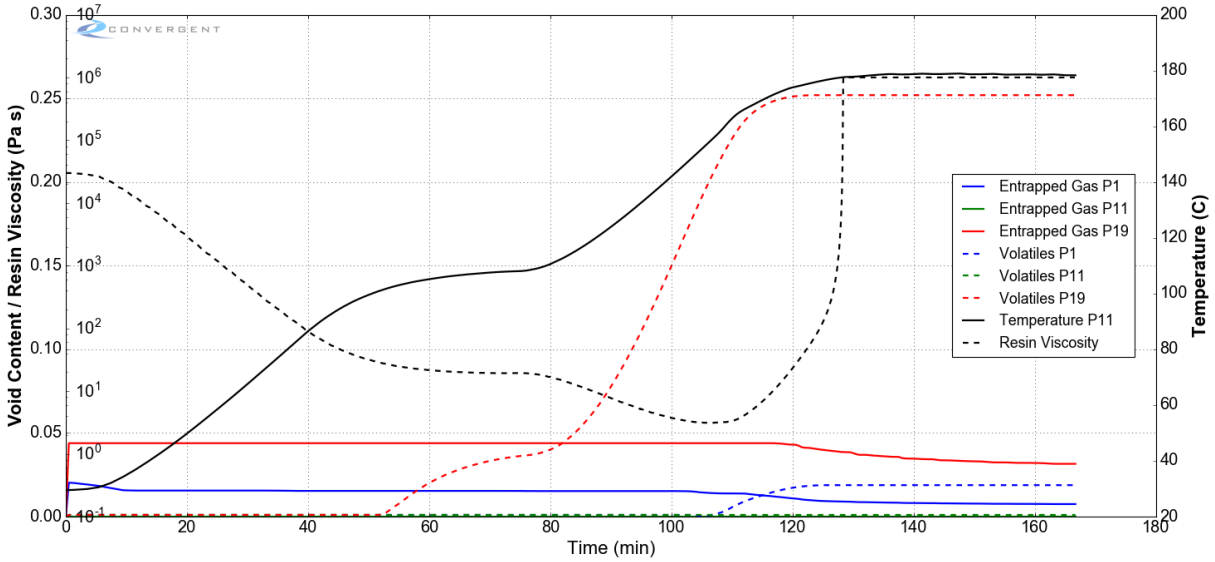

Figure 12. Evolution of the void content contributions in test 3 from entrapped gas (solid lines) and volatiles (dashed lines) over the representative sensors P1, P11, and P19

Shown below in Table 3 is a summary of the measured porosity at each location of interest in the experimental tests and the predicted porosity values from simulation. The trends observed in experiments are captured in the simulation, further refinement of simulation parameters is necessary to quantitatively match the measured values. The primary range of interest for refinement is a final porosity of 0.0-5.0%, above this range any amount of porosity is too severe for industry requirements. Based on this requirement, it is clear that maintaining pressure throughout the cycle and mitigating off-gassing is necessary for achieving a reasonable porosity level and therefore this modeling framework is valuable for identifying zones of high risk due to pressure shielding.

Table 3. Comparison summary of the porosity observed in experiments and simulations (total porosity)

	P1		P11		P19	
	Test (%)	**Sim. (%)**	**Test (%)**	**Sim. (%)**	**Test (%)**	**Sim. (%)**
Test 1 (no caul sheet)	0.12	0.00	0.11	0.10	0.24	0.10
Test 2 (0.32 cm caul)	0.32	0.00	0.58	0.10	0.82	4.17
Test 3 (1.27 cm caul)	0.63	2.60	0.61	0.10	12.15	28.34

*Simulation void volume fraction is the total void fraction from the three sources considered

4. CONCLUSIONS

The Integrated Flow-Stress 3 Phase framework discussed in previous work has been extended to include the evolution of volatiles due to off-gassing. The scope of this model development includes the diffusion of moisture dissolved in resin to voids and evaporation leading to void growth. Test panels with ply drops were manufactured using different caul sheet configurations to assess the likelihood of porosity due to the variations in local resin pressure. Micrographs of the panels were taken from representative locations to evaluate the range of local pressures expected. Simulations of the experimental tests were built using Convergent Manufacturing Technologies IFS3P* framework within COMPRO-Abaqus 2018. Simulations were designed using the coupled

thermal-consolidation framework with the implemented off-gassing capability. The current tools enable qualitative prediction of porosity due to entrapped and volatiles off-gassing.

5. ACKNOWLEDGMENTS

This work was performed under the sponsorship of the National Aeronautics and Space Administration under NASA Project ID: NNL16AA09C. The authors would like to thank Convergent Manufacturing Technologies for supplying the resin pressure sensors and expertise on the test method and data reduction.

6. REFERENCES

1. J. Wells, “Behaviour of Resin Voids in Out-of-Autoclave Prepreg Processing,” Master’s Thesis, The University of British Columbia, 2015.
2. L. Farhang, “Void evolution during processing of out-of-autoclave prepreg laminates,” PhD Thesis, The University of British Columbia, 2014.
3. H. Bedayat et al., “An Efficient Modelling Approach for Prediction of Porosity Severity in Composite Structures,” Proceedings of the 2017 Society for the Advancement of Material and Process Engineering (SAMPE) conference. Seattle, WA.
4. H. Bedayat et al., “Numerical and Experimental Study of Local Resin Pressure for the Manufacturing of Composite Structures and the Effect on Porosity,” Proceedings of the 2018 Society for the Advancement of Material and Process Engineering (SAMPE) conference. Long Beach, CA.
5. S. A. Niaki, A. Forghani, R. Vaziri, and A. Poursartip, “A two-phase integrated flow-stress process model for composites with application to highly compressible phases,” Mech. Mater., vol. 109, pp. 51–66, 2017.
6. S. Amini Niaki, “A three-phase integrated flow-stress framework for process modelling of composite materials,” PhD Thesis, The University of British Columbia, 2017.
7. S. A. Niaki, A. Forghani, R. Vaziri, and A. Poursartip, “A three-phase integrated flow-stress model for processing of composites,” Mechanics of Materials, 2017.
8. M. Roy, J. Kay, G. Fernlund, and A. Poursartip, “Porosity in Configured Structures,” Proceedings of the 2015 Society for the Advancement of Material and Process Engineering (SAMPE) conference. Baltimore, MD.
9. M. Roy, “Porosity in configured structures : effect of ply drops and caul sheets in the processing of composite parts,” Master’s Thesis, University of British Columbia, 2015.
10. J. Wood and M. Bader, “Void Control for Polymer-Matrix Composites (1): Theoretical and Experimental Methods for Determining the Growth and Collapse of Gas Bubbles,” Composites Manufacturing, Vol. 5 No. 3. 1994.
11. J. Wood and M. Bader, “Void Control for Polymer-Matrix Composites (2): Experimental Evaluation of a Diffusion Model for the Growth and Collapse of Gas Bubbles,” Composites Manufacturing, Vol. 5 No. 3. 1994.

12. S. M. Haghshenas, “Integrating resin flow and stress development in process modeling of thermoset composites,” PhD Thesis, The University of British Columbia, 2012.
13. M. A. Biot and D. G. Willis, “The elastic coefficients of the theory of consolidation,” J. Appl. Mech., vol. 24, pp. 594–601, Jan. 1957.
14. J. R. Rice and M. P. Cleary, “Some basic stress diffusion solutions for fluid-saturated elastic porous media with compressible constituents,” Rev. Geophys., vol. 14, no. 2, p. 227, 1976.
15. M. A. Biot, “General theory of three-dimensional consolidation,” J. Appl. Phys., vol. 12, no. 2, p. 155, 1941.
16. P. Hubert, “Aspects of flow and compaction of laminated composite shapes during cure,” PhD Thesis, The University of British Columbia, 1996.
17. P. Hubert, R. Vaziri, and A. Poursartip, “A two-dimensional flow model for the process simulation of complex shape composite laminates,” Int. J. Numer. Methods Eng., vol. 44, no. 1, pp. 1–26, Jan. 1999.
18. R. Lewis and B. Schrefler, Finite Element Method in the Deformation and Consolidation of Porous Media. 1998.
19. Convergent, “COMPRO.” Vancouver, BC, Canada, 2017.